Journal of Advanced Joining Processes 1 (2020) 100008

Contents lists available at ScienceDirect

Journal of Advanced Joining Processes

journal homepage: www.elsevier.com/locate/jajp

Bonding mechanisms in laser-assisted joining of metal-polymer composites

K. Schricker[a,*], L. Samfaß[a], M. Grätzel[a], G. Ecke[b], J.P. Bergmann[a]

[a] Technische Universität Ilmenau, Department of Mechanical Engineering, Production Technology Group, Gustav-Kirchhoff-Platz 2, 98693 Ilmenau, Germany
[b] Technische Universität Ilmenau, Department of Electrical Engineering and Information Technology, Nanotechnology Group, Gustav-Kirchhoff-Platz 2, 98693 Ilmenau, Germany

ARTICLE INFO

Keywords:
Laser-based metal plastic joining
Hybrid joints
Metal thermoplastic joining
Thermal joining
Bonding mechanism

ABSTRACT

Metal-Plastic hybrid components and assemblies are gaining importance due to novel lightweight constructions and a growing integration of functions by using the right material at the right place. Thermal joining enables a joining technology for thermoplastic materials and engineering metals without using adhesive or joining elements. The paper provides novel investigations on the interaction between form fit and physicochemical interactions due to the combined use of specifically used oxide layers, interaction barriers and defined surface structuring by laser processing. Thereby, the design of experiments allows the investigation of the form fit as dominant interaction mode.

Introduction

Composite structures are gaining importance in different industries due to the advantages of multi-material constructions. The use of such components reaches far beyond automotive industry and lightweight design as single motivation. For example, the white goods industry is realizing many hybrid joints for increasing the level of functions within a component as well as a high-quality appearance, e.g. metal panels on injection moulded parts. This industry reaches large scale volumes at the level of millions of pieces a year. Thereby, innovative joining processes for realizing multi-material constructions on short processing times are necessary for an economically viable production.

Thermal direct joining of thermoplastic components with technical metals is a modern technique for realizing hybrid composites without the need of joining elements (e. g. screws, rivets) or additional components (e. g. adhesives) to reduce the number of process steps and cycle times. In thermal joining, the metal sheet and the thermoplastic component are clamped and in contact at the boundary layer. By starting the process, the metal sheet is heated due to the energy input and a heat flux between both joining partners occurs. This leads to a melting layer of thermoplastic material at the boundary layer. The molten material wets the metal surface and penetrates the structures of the metal surface. After solidification of the molten thermoplastic material, a permanent joint is formed. This process can be performed by different energy sources, e. g. laser irradiation (Katayama et al., 2007), resistance heating (Ageorges and Ye, 2001) or friction joining (Amancio-Filho et al., 2011). A laser-based process shows advantages due to a geometrically independent and locally limited energy input. Thereby, the process can be performed as transmission joining or heat conduction joining. In transmission joining, the laser beam is transmitted through the plastic sheet as upper joining partner and the laser irradiation partially absorbed at the metal surface. The polymer gets molten through the heat transfer at the interface and forms a joint as described. In heat conduction joining, the metal sheet is used as upper joining partner and the laser beam is targeted to the surface. The heat is conducted through the metal sheet into the boundary layer and joining zone. In contrast to transmission joining, the transmissivity of the thermoplastic material within laser wavelength is not necessary and a high thermal load of the thermoplastic due to the absorption of the laser beam at the contact area can be avoided.

Numerous investigations were carried out regarding different aspects of laser joining metals with thermoplastics. In terms of bonding mechanisms, (Kawahito and Katayama, 2010) and (Arai et al., 2014) detected a firmly bonding between metal and plastic. Especially the influence of oxide layers in combination with different thermoplastic materials were discussed by several authors. Depending on the thermoplastic structure and polarity, a significant influence on mechanical properties and firmly bonding was shown. (Lamberti et al., 2014) documented a positive influence on joint formation between aluminum oxide layers and polyamides by physicochemical interactions, especially hydrogen bonds. (Jung et al., 2016) showed that the thickness of a zinc oxide layer on steel is proportional to the joint strength for joints with ABS. (Zhang et al., 2016) describes the effect of anodized aluminum surfaces regarding shear strength, whereby a positive effect of the oxide layer with oxygen contents up to approx. 14% are met. Positive effects of oxide layers are also discussed in (Katayama and Kawahito, 2008), (Katayama et al., 2007) and (Tan et al., 2013). Besides the firmly bonding, (Markovits et al., 2012) demonstrated the influence of mechanical interlocking to achieve a higher loadability of the joint. Surface preparation of the metal sheet is used to obtain a suitable mechanical interlocking. Various surface preparation methods were

* Corresponding author.
E-mail address: klaus.schricker@tu-ilmenau.de (K. Schricker).

https://doi.org/10.1016/j.jajp.2020.100008
Received 11 November 2019; Received in revised form 15 January 2020; Accepted 15 January 2020

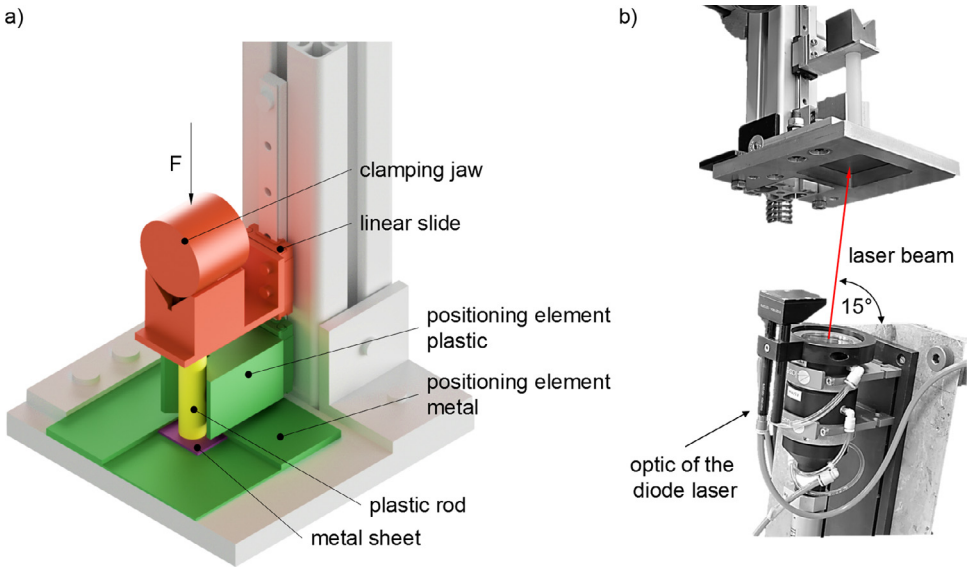

Fig. 1. Schematic view on clamping device (a) and experimental setup for heat conduction joining process (b).

investigated such as laser-based processes (Amend et al., 2014; Heckert and Zaeh, 2014), chemical etching (Hino et al., 2011), corundum blasting (Bergmann and Stambke, 2012) and machining (Cenigaonaindia et al., 2012; Schricker et al., 2014). Independent of the structuring process, structure density and a high number of undercuts showed the highest influence on the joint strength. Furthermore, the investigations by (Schricker and Bergmann, 2019), showed that the temperature distribution in the melting layer of the polymer has a decisive influence on the structure filling. The melting interval must be completely passed through in order to fill the surface structures safely and independently of the joining time. It is also important that the achievable mechanical properties do not depend on the melting layer thickness insofar as a sufficient quantity of molten material is provided to completely fill the surface structures (Schricker et al., 2016). In addition, a force fit between both materials is a possible effect on joint strength as well and was briefly alluded in (Flock, 2011) and (Paul et al., 2014) based on different thermal expansion coefficients between the materials. Several effects may interact and a strict separation of the different components in the bonding mechanism (form fit, firmly bonding, force fit) is not provided within the state of the art. Since the influencing variable of force fit is time-dependent due to relaxation, the effect is not considered in the following investigations and will be described at a later point in time.

This paper focusses on the interaction between firmly bonding and form fit. For this purpose, different polymers were used, and multiple interlayers are specifically applied to the boundary layer. This allows the adhesive forces to be altered by the chemical composition of the interface and the structure of the polymers in order to determine the influence of the bonding mechanisms on the tensile strength. Finally, firmly bonding and form fit are superimposed in order to quantify the influence at different structural densities.

Experimental setup

The joining process was performed using a fiber-coupled diode laser (Laserline LDM 1000, P_{max} = 1000 W, λ = 980 nm). Due to the research based on fundamental aspects, the joining process was carried out for spot joints of thermoplastic rods on metal plates. The clamping device and the experimental setup are shown in Fig. 1. A polymer rod is positioned within the setup on a metal sheet and clamped by a defined mass (a). The process is realized as heat conduction joining, wherefore the laser optic is positioned below the clamping device (b). This setup allows a heat conduction joining and then a tensile test in order to compare the different surface conditions. The joining pressure was set to 0.1 Nmm^{-2} by preliminary investigations.

Table 1
Joining parameters for the following investigations.

Polymer	Metal	Laser beam power P_L (W)	Joining time t_L (s)
PA 6	AISI 304	100	16
PP	AISI 304	100	18
PA 12	AISI 304	100	16

The joining times (t_L) were varied from 5 s up to 28 s in preliminary investigations in order to achieve a homogeneous melting layer thickness for each material. Due to the fact that the investigations address fundamental aspects of the bonding mechanism, no optimization of the joining time was pursued. On the other hand, a long joining time in combination with a homogeneous temperature distribution allows the formation of a uniform melting layer in the polymer. Therefore, the joining process was carried out with a constant laser beam power of 100 W (intensity: 3.5 W mm^{-2}, rectangular spot shape, spot size: 17·17 mm^2, top hat intensity profile). The rectangular laser spot irradiates almost the whole metal sheet to meet the requirements for setting the required temperature field.

The high alloyed steel AISI 304 (t = 1 mm, width = 15 mm, length = 20 mm) was applied as metal joining partner. The polymer rod has a diameter of 10 mm and a length of 70 mm, which is independent of the material. Polypropylene (PP) and polyamide 6 (PA 6) were used due to their different chemical structure resulting in different material properties. These plastics were selected because of their different polarity and chemical structure. PP as a nonpolar plastic serves as a reference for the pure form fit. In contrast, PA 6 differs in the structure and can form hydrogen bonds (Krevelen van and Nijenhuis, 2009). Therefore, adhesion forces between plastic and metal form during thermal joining. By comparing the two polymers and using different interlayers, it is possible to distinguish between form fit and firmly bonding. It should be noted that other material properties also differ, e. g. melting temperature and viscosity. However, the use of sufficiently high temperatures and long joining times can minimize such an influence on joint formation. Finally, studies were carried out on PA 12 to verify the results.

The joining parameters given in Table 1 were selected in preliminary investigations by considering the uniformity of the melting layer thickness by the minimum associated standard deviation for each material. In addition, the uniformity of the melt ejection by comparing its height

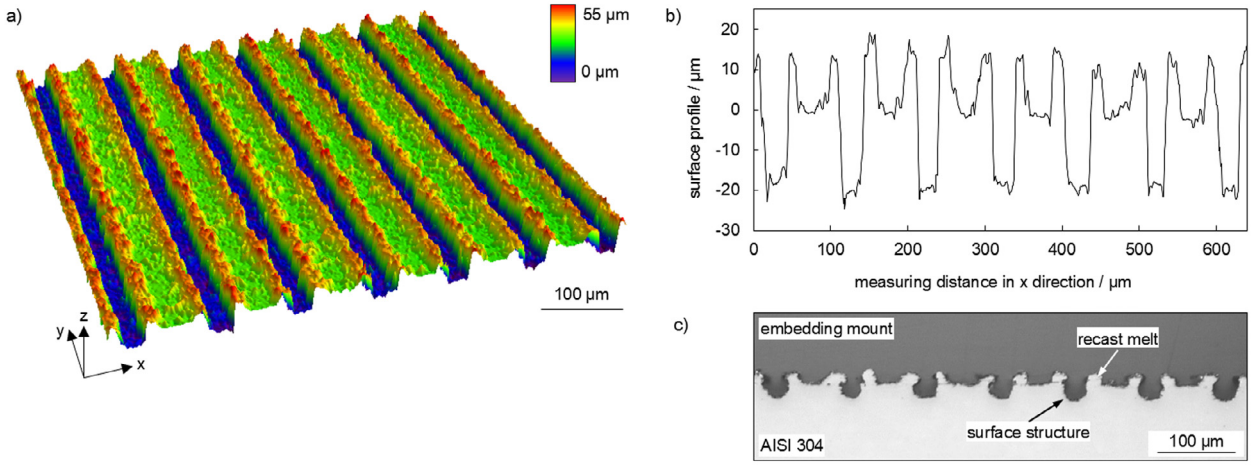

Fig. 2. Laser-based surface preparation in LSM microscopy (a), surface profile (b) and microsection (c).

and maximum expansion was also evaluated. Therefore, the joining parameters with the most uniform appearance of the joining zone were applied individually for each material in these investigations. The plastic rod is connected to the metal over the entire cross-section for PA 6 as well as for PP and a visible degradation is avoided despite the long joining times. A detailed description of the joining zone for the selected parameters is given in chapter 3.

The metallic surface is of great importance for the joining process. On the one hand, the physicochemical interactions are dependent on it, on the other hand because the form fit can be produced via the structuring of the metal surface. The sheets are used both unstructured and structured condition. In these two cases, they are cleaned for 5 min with acetone and isopropanol in an ultrasonic bath, then rinsed with distilled water and dried with air. In order to support the form fit, groove structures as shown in Fig. 2 were manufactured by a pulsed fiber laser process (Rofin PowerLine F20, $P = 18$ W, $f = 60$ kHz, v = 200 mm·min^{-1}). The geometry of the grooves as well as the orientation of the structures were kept constant, as no effect is to be expected due to the rotationally symmetrical joining zone and the tensile test of this specific joint configuration. Using a pulsed laser beam process, reproducible surface structures can be created which ensure a high surface enlargement and the repeatable formation of undercuts due to melt ejection and recast. Furthermore, the structure density can be easily adjusted by varying the distance between the grooves.

In order to control the interaction between the firmly bonding and the form fit, different coatings were applied to the surfaces (structured/unstructured) to act as an interlayer between plastic and metal at the boundary. The coatings were manufactured with the Ardenne PVD-Cluster CS 400 ES system for DC magnetron sputtering. Thereby, the sputtering targets are inclined 30° to the substrate. The substrate and targets are tilted and additionally eccentrically arranged to each other. This design and the rotation of the substrate during processing (15 min^{-1}) obtains the production of homogeneous coatings which can also achieve undercuts and pits. Chromium layers with a thickness from 25 nm up to 100 nm were manufactured and expected to form oxides for an improvement of the adhesion forces. Furthermore, carbon layers with a thickness from 10 nm up to 30 nm were used as a physicochemical interaction barrier between the joining partners and are manufactured in a PVD process as well. The process parameters used for the sputtering process are given in Table 2. It should be noted that a limitation of the parameter windows was carried out in advance through preliminary investigations. The layer thicknesses deviate by approx. ± 5% and are adjusted to the deposition rate based on reference tests.

Mechanical testing was carried out by tensile test (test speed = 10 mm·min^{-1}, universal testing machine Zwick 1455) to gain

Table 2
Parameters for DC magnetron sputtering.

Coating	Power (W)	Argon flow rate (sccm)	Process pressure (mbar)	Sputter rate (nm s^{-1})
chromium	50	30	$5{\cdot}10^{-3}$	0,11
Carbon	500	30	$5{\cdot}10^{-3}$	0,1

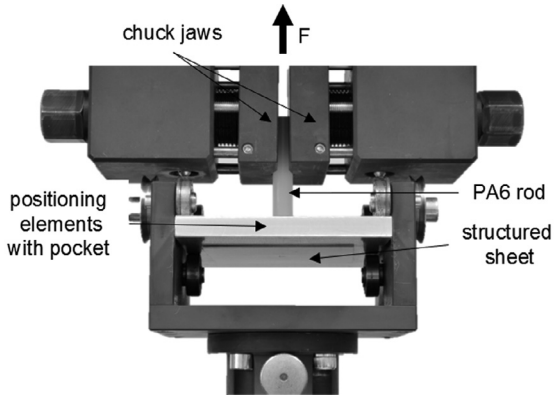

Fig. 3. Setup for tensile test.

information on the resulting joint strength. The test setup (Fig. 3) allows the direct comparison between different surface modifications as shown in (Kohl et al., 2018). Due to the fact that the water absorption of polyamides influences the mechanical properties, there is a period of seven days between joining and testing for all samples. In addition, the possible influence of the force fit on the result can be kept constant. The tensile strength was calculated from the maximum tensile force divided by the nominal connecting surface of the rod. The sample size (n) is at least three for statistical validation of the tests. The error bar in all diagrams represents the standard deviation.

Microsections were taken out of the middle of the joining zone for materialographic investigations. For further investigations, scanning electron microscopy (SEM, Hitachi SEM S4800) and laser scanning microscopy (LSM, Olympus LEXT 4000) were used. Auger electron spectroscopy (AES) depth profiling was performed to investigate the elemental composition profiles of the formed layers using a Thermo VG Scientific Microlab 350 instrument. The spectra were acquired at an accelerating voltage of 10 keV and a primary electron beam current of 3 nA and a beam diameter of approximately 30 nm with an incident

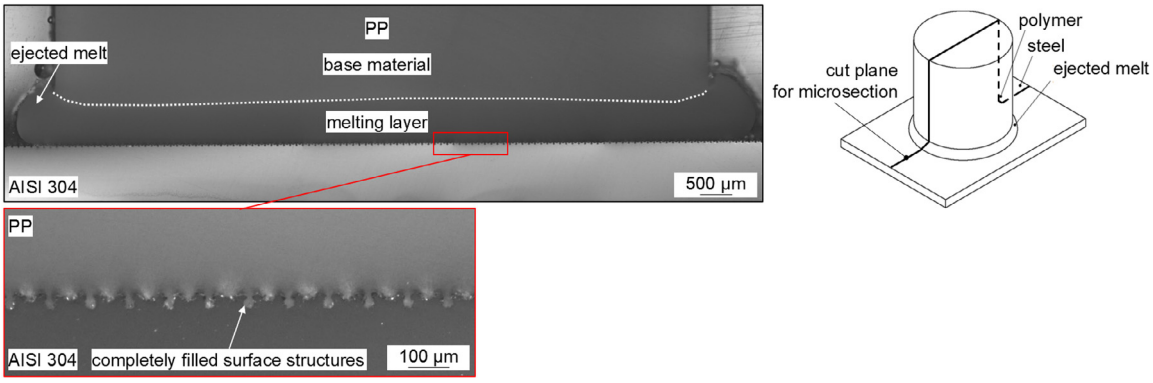

Fig. 4. Joining zone of a PP-AISI 304 joint (t_L = 18 s).

Table 3
Auger peaks for the major constituent elements.

Element	Auger transition	Augerpeak position (eV)	Measured range (eV)	Sensitivity factor (1)
C	KLL	~262	240–300	0.6
O	KLL	~514	460–545	0.96
Cr	$M_{2,3}VV$	~38	30–170	–
Cr	$L_3M_{23}M_{23}$	~491	440–800	–
Cr	$L_3M_{23}M_{45}$	~529	460–545	0.29
Fe	$L_3M_{23}M_{45}$	~650	630–720	0.46
Fe	$L_3M_{45}M_{45}$	~704	630–720	–
Ni	$L_3M_{23}M_{45}$	~775	750–870	–
Ni	$L_3M_{45}M_{45}$	~848	750–870	0.6

angle of 60° with respect to the surface normal. The surface was rastered during the measurement over an area of some square microns. The measurement was carried out by a concentric hemispherical analyzer (CHA) and a detection angle of 0°. The energy resolution of the detector was 0.25%. The Auger spectra were detected with a step width of 0.7–0.8 eV and a dwell time of 150–200 ms. Sputtering was carried out using a 1-K eV Argon ion beam of approx. 700 nA over an area of 2·2 mm^2 and an incident angle of 43.4°. The base pressure in the analysis chamber was $1{\cdot}10^{-9}$ mbar. The depth profiling was carried out and the Auger intensities of the major constituent elements in the layer were evaluated. For all the specimens, the mean values of the Auger peaks monitored are given in Table 3. Some Auger signals were used for quantification of the depth profiles. In case of O and C only one peak can be used for that purpose. For Cr and Fe only one suited peak was used for the quantification. For these peaks the sensitivity factors from the spectrometer software Avantage is listed in the last column.

Results and discussion

Description of the joining process and the initial situation

At the beginning, the results for the joining zone between polymer and metal are presented on the basis of the performed process. It is essential to achieve a uniform melting layer and melt ejection in the plastic to obtain a constant connection over the entire cross-section of the plastic rod. Fig. 4 shows this exemplarily for an AISI 304-PP joint. The thickness of the melting layer is almost constant, there is no significant maximum in the middle of the rod. The slight increase of the melting layer thickness in the direction of the shell surface of the rod is due to a heat accumulation at this point because of the varied heat transfer to the environment. The melt ejection is also very uniform. This indicates that there is a very homogeneous temperature distribution and a consistently good connection is created over the entire cross-section between polymer and metal. The detail image within the microsection demonstrates the high number of undercuts created by the laser-based preparation of the metal surface and shows that these structures are completely filled with polymer. Therefore, a high form fit is achieved. It should be noted that the different shades of gray follow from the optically translucent properties of the polymer in interaction with the illumination in microscopy.

To this point, it was shown that the experimental setup can produce the required uniform joining zone. A detailed analysis of the melting layer is carried out for the investigated polymers to give a further description of the joining zone.

Fig. 5 shows the dependency of the melting layer thickness over the diameter of the polymer rod for the selected parameters. For the plastics considered, the thickness of the melting layer is relatively uniform and is equivalent to the characteristics described. However, a large dependency on the thermophysical properties can be determined, in particular the melting temperatures. These rise from PP (approx. 160 °C) to PA 6 (approx. 220 °C). Correspondingly, the thickness of the melting layer also decreases with increasing melting temperature. The differences in the melting layer thickness do not follow the difference in the melting temperatures linearly, since other relevant material properties also vary, in particular thermal conductivity, density, specific heat capacity and melting enthalpy. A detailed consideration of these influencing variables can be found in (Schricker and Bergmann, 2018). Furthermore, the different joining times of 18 s for PP and 16 s for PA 6 also affect the melting layer thickness. With the same joining parameter as for PA 6, the melt zone thickness of PP would be reduced by approx. 50 µm to approx. 640 µm in the center of the joining zone.

The already mentioned aspect of the uniform temperature distribution within the joining zone, which is reflected in the evenly formed melting layer of PA 6 and PP. An adapted numerical simulation according to (Schricker et al., 2015) also showed that the polymer is completely molten at the interface, which supports the complete penetration of the surface structures. Moreover, the decomposition temperature is not reached for any of the parameters used.

For a detailed consideration of the mechanical properties, Fig. 6 shows the tensile strength as a function of the polymer as well as the surface configuration of AISI 304 (structured/unstructured). For the unstructured metal, average tensile strengths of approx. 2.1 MPa are achieved for PA 6. At the same time, the percentage of form fit in the bonding mechanism of the unstructured surface is of minor importance, since no connection can be achieved for PP. SEM images of the unstructured metal surface illustrate this, as the rolling texture is only formed on small scales of several hundred nanometers and no sufficient mechanical interlocking is reached. For the structured sheet metal, significantly increased joint strengths are gained for both polymers due to the rough, fissured and substantially enlarged surface. The polyamide reaches a tensile strength level in the range of 11.3 MPa. PP now also achieves tensile strengths in the range of 8.7 MPa due to the form fit. The strength is lower than with polyamides, as the strength of the base

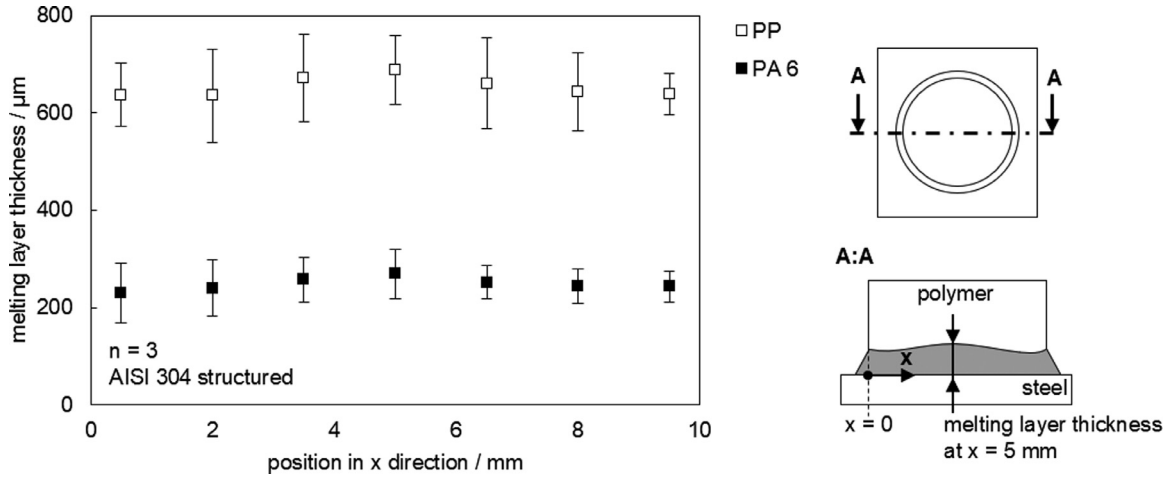

Fig. 5. Melting layer thickness over the width of the polymer rod ($t_{L,PP}$ = 18 s, $t_{L,PA\ 6}$ = 16 s).

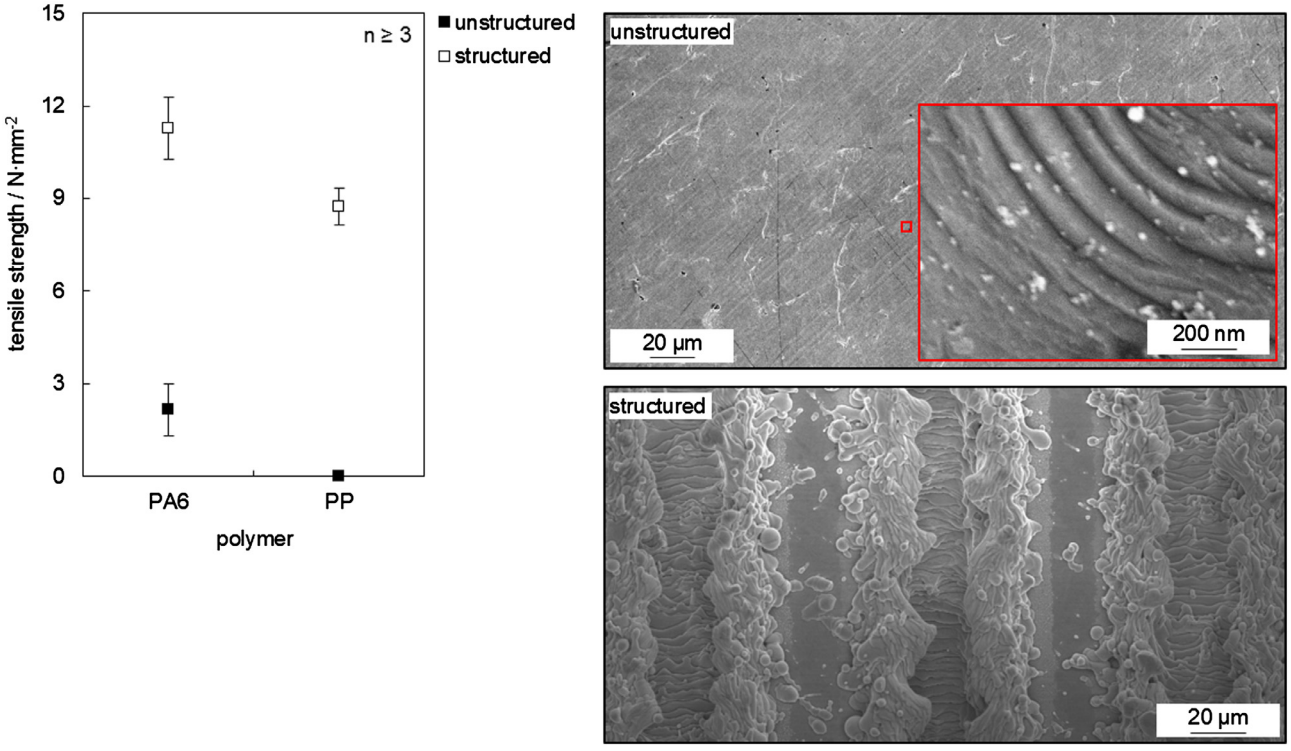

Fig. 6. Tensile strength of different polymers depending the surface preparation and corresponding SEM images of the unstructured and the structured surface before joining.

material is already reduced compared to polyamides (PP: approx. 30 MPa, PA 6: approx. 75 MPa).

However, the fracture surface clearly shows that the initial strength of the plastics is only partially relevant or cannot be fully utilized. For polyamides, a mixed fracture with cohesive and adhesive fracture components is evident in all cases. For the structured sheets, material residues remain also within the grooves of the surface structure for all considered polymers (Fig. 7a and b). A clear difference in the percentage of fracture cannot be determined for the different polymers. It should be noted that the fracture pattern also shows that the area of ejected melt does not contribute significantly to the bond strength, given that the grooves of the surface structure are not apparent. Micrographs have confirmed this finding.

The temperatures in the joining zone are low enough to prevent the formation of bubbles due to decomposition as described in (Schricker et al., 2018). The bubbles that occur can therefore be attributed to the moisture in the polyamide. The bubbles of the polyamide are partially transported into the melt ejection due to the flow of molten polymer caused by the joining pressure. The remaining bubbles in the inner area of the joining zone appear a few tens of micrometers above the interface. In these areas, a cohesive failure of the polymer occurs due to the reduced cross-section. The underlying structures remain completely filled with plastic (Fig. 7c). It should be noted that no systematics for the increased occurrence of bubbles in a certain area of the joining zone could be determined, even if the fracture pattern shown in Fig. 7b would indicate that differently.

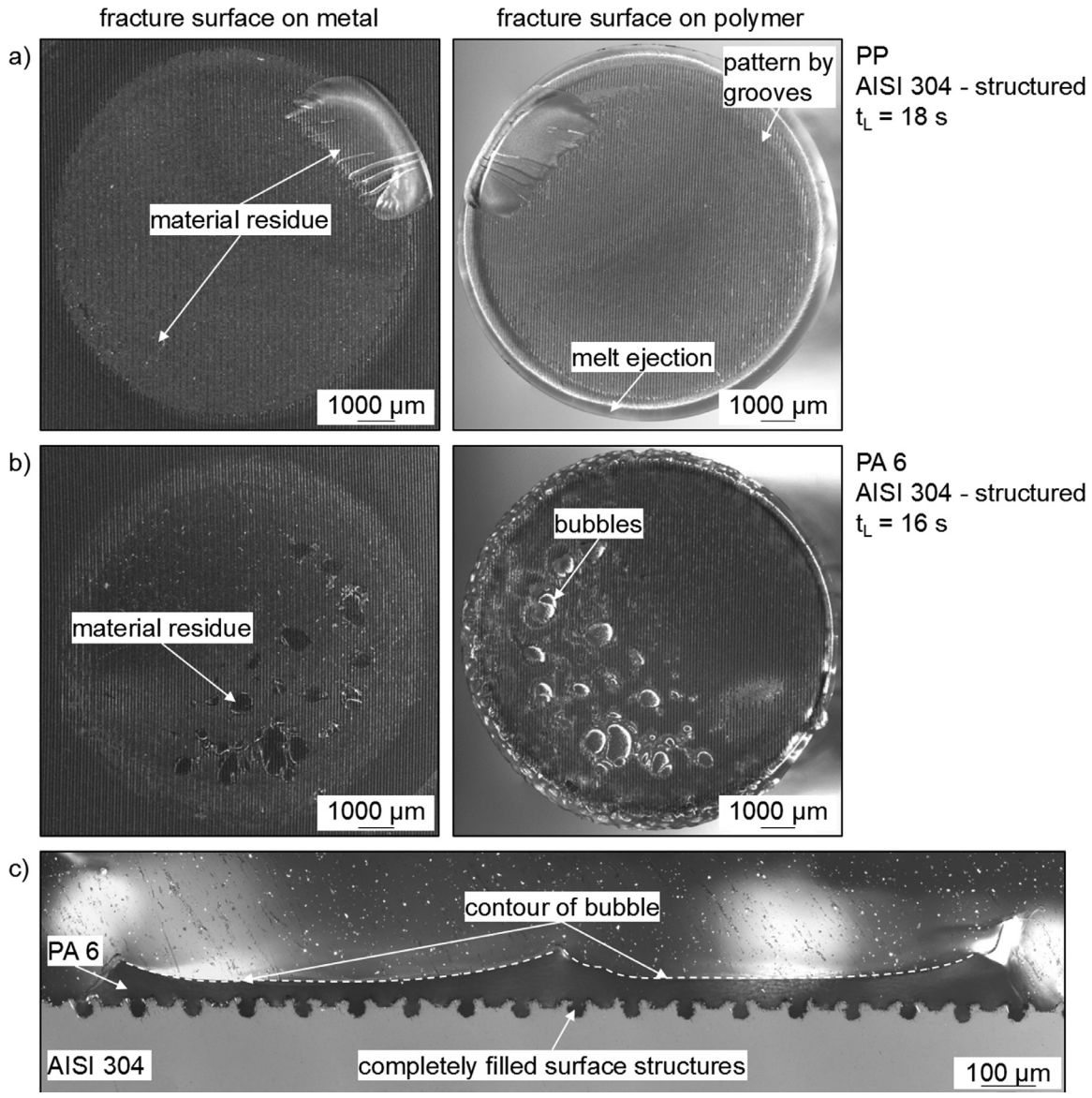

Fig. 7. Fracture surface on metal and polymer after tensile test for structured AISI 304 with PP (a), PA 6 (b). Microsection of fracture surface with material residue under bubbles (c).

Side studies showed no influence of a drying of the polyamides before joining on the resulting tensile strength despite a reduction of the bubble formation. For this reason, the industrial application of the process does not require drying prior to joining.

On this basis, further investigations can be carried out, in particular to determine the role of the different mechanisms of action, i.e. form-fit and firmly bonding. This requires a separate consideration of these influencing variables in the first step. In order to adjust the adhesion forces, interlayers are therefore applied to the interface on a nanometer scale, on the one hand to improve or switch off the physicochemical interactions and, at the same time, to influence the surface structures as little as possible.

Effect of interlayers on firmly bonding

In order to evaluate the influence of the interlayers on the firmly bonding, unstructured sheets are considered at the beginning. Chromium layers are used to improve the joint strength due to an increase of adhesion forces by the interactions between the chromium oxide and the polar PA 6. Fig. 8a shows the relationship between tensile strength and interlayer thickness from 25–100 nm. As expected, no connection between chromium oxide and PP was achieved. This also shows that no significant mechanical interlocking can be reached with the chromium oxide. PA 6 achieves comparable average strengths of approx. 6.1–6.9 MPa for interlayer thicknesses in the range from 25 nm to 50 nm, where the second has the smaller standard deviation. The strength of approx. 7 MPa is factor 3.3 compared to the original surface without an interlayer. From 75 nm, the standard deviation increases significantly and the mean tensile strength drops to a considerably lower level of approx. 4.1 MPa until no tensile strength is reached at 100 nm.

The fracture patterns provide some indications for this behavior. From a layer thickness of 25 nm, a mixed fracture occurs (Fig. 8a). The exemplary image for 50 nm shows the residual chromium on the plastic after the tensile test. A further increase of the interlayer thickness leads to larger areas of adhesive failure between chromium interlayer and the AISI 304 substrate. An almost fully adhesive failure occurs at 100 nm layer thickness. SEM investigations (Fig. 8b) have shown that the morphology of the chromium layer reveals cracks for interlayer thickness of 75 nm onwards, while thinner layers are undamaged. These cracks act as weak points and grow significantly with increasing layer thickness,

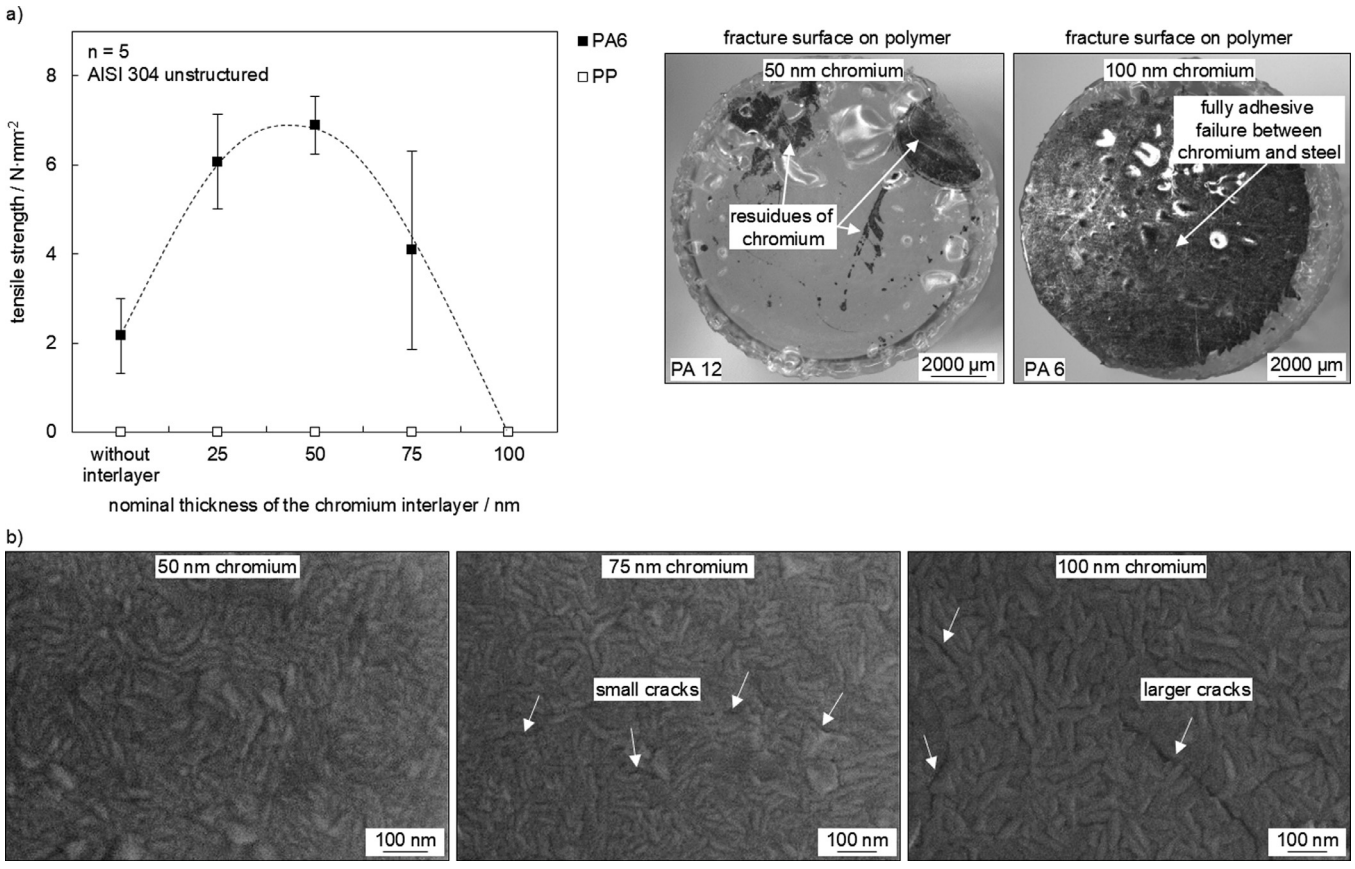

Fig. 8. Effect of chromium interlayers on tensile strength and fracture pattern (a) and SEM images of different thicknesses of the chromium coating at the metal surface (b).

ultimately leading to complete adhesive failure between interlayer and substrate. It should be noted that the interlayer thicknesses examined in the SEM suggest that the applied layers are continuously formed, which means that the surface is covered with chromium completely.

In case the interlayer is intact, its thickness plays a subordinate role regarding the joint strength. This behavior can be explained by the chemical composition of the interlayers compared to the base material by Auger electron spectroscopy (AES). This method enables the chemical composition of a surface to be investigated on a scale of nanometers by a stepwise ablation with an electron beam. The results for an interlayer thicknesses of 25 nm and the base material depending the sputtering time are given in Fig. 9. A greater depth is reached with increasing sputtering time. Due to the transition from the coating to the base material, the alteration in the chemical composition leads to a change in the ablation rate, therefore the depth is not specified in order to depict a reliable result.

In case of the interlayer shown in Fig. 9a, it is well recognizable that it essentially consists of chromium and that oxygen accumulates mainly in the near surface region due to the formation of chromium oxides. The interlayer thickness is well recognizable over the sputtering time. The high level of carbon on the surface is a typical effect due to the almost unavoidable contamination by organic substances, e. g. when samples are in contact to plastics during storage. It appears that the interlayer is continuously formed, as already assumed in the SEM picture, because iron is only found at greater depths when the chromium level drops to the level of the base material. In addition, the oxygen level within the chromium coating drops close to zero as seen in the example of 25 nm. If the layer is not continuous, diffusion processes could cause an increased content of other elements in this area. Furthermore, in addition to the oxygen peak at the surface, a second peak at the transition into the base material can be determined at sputtering times of approx. 175 s for 25 nm. This peak is caused by the natural oxide layer of the AISI 304 and more broadly pronounced compared to the peak at the surface. This can be attributed to a different surface roughness during ablation with the electron beam and a varied ablation rate because of the different material composition. In addition, the coating process can affect the chemical composition of this transition zone, e.g. by impact of argon ions at the beginning of the sputtering.

Therefore, a comparison between an uncoated reference (Fig. 9b) and the interlayer is given. The measured oxygen content on the reference surface is even higher than on the surface of the chromium coating with approx. 27% compared to approx. 20%. This implies that the absolute oxygen content is not decisive for the bond strength. On the other hand, a fundamentally changed chemical composition can be seen in the area close to the surface. For all investigated interlayers, this area consists mainly of chromium, oxygen and carbon. In contrast, the chromium content of the base material is massively reduced at this point, whereas a large proportion of iron and a small amount of nickel is present. With increasing depth, the chemical composition then approaches the composition typical for this alloy (approx. 18% Cr, approx. 10% Ni). This indicates that the chemical composition of the surface area as a whole has a significant effect on the achievable joint strength. It can be assumed that, due to the high chromium content in combination with oxygen, chromium oxides predominate on the surface of the interlayer, which is why the bond strength can be increased compared to the starting material.

Furthermore, between the interlayer thicknesses of 25 nm and 50 nm, the chemical composition of the surface area is comparably formed, which is why the increase in tensile strength is achieved regardless of the thickness of the coating.

In addition to an improvement of the adhesion, the complete avoidance of physico-chemical interactions is also of relevance for the

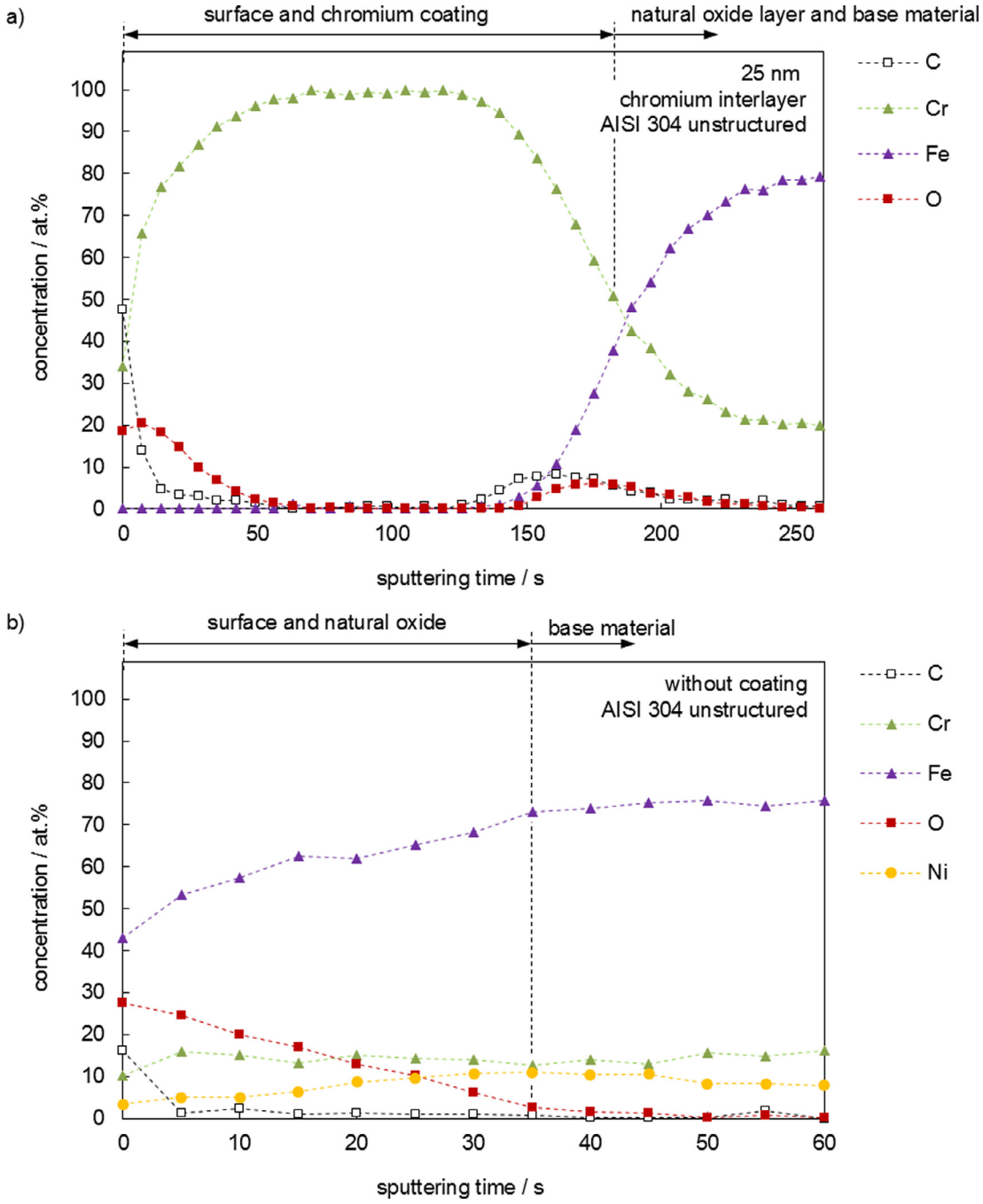

Fig. 9. AES results for an interlayer thickness of 25 nm (a) and an uncoated reference (b) on unstructured AISI 304.

following considerations. The role of an interaction barrier is to be achieved by carbon coatings. Fig. 10 shows the tensile strength over the carbon interlayer thickness. While PP, as expected, shows no connection, the tensile strength of PA 6 decreases with increasing layer thickness. At 10 nm the tensile strength is significantly reduced, although a layer of 10 nm thickness should already produce a much greater range than the chemical or physical bond lengths can bridge (≪1 nm) (Lee, 1991). However, continuously formed and thus completely closed interlayers are not achieved for thicknesses of 10 nm, which is why adhesion forces can still be acting. The required layer thicknesses are thus significantly higher than the average bond lengths. At 30 nm there are no acting adhesion forces between plastic and metal left, thus no plastic-metal joint is produced. The fracture surfaces also show a complete detachment of the carbon layer from the substrate (Fig. 10).

However, by means of a SEM investigation it can be verified that the interlayers for chromium at 50 nm and carbon at 30 nm are completely closed respectively continuously formed (see also chapter 3.3).

At this point it can be concluded that an improved connection is achieved for chromium interlayers. Due to the lower standard deviation in tensile testing, the following investigations are performed for chromium interlayer thicknesses of 50 nm. On the other hand, the impact of adhesion forces can be eliminated by using carbon coatings with a thickness of 30 nm. Both are applied as interlayers to laser-structured surfaces in order to specifically promote or eliminate adhesion forces.

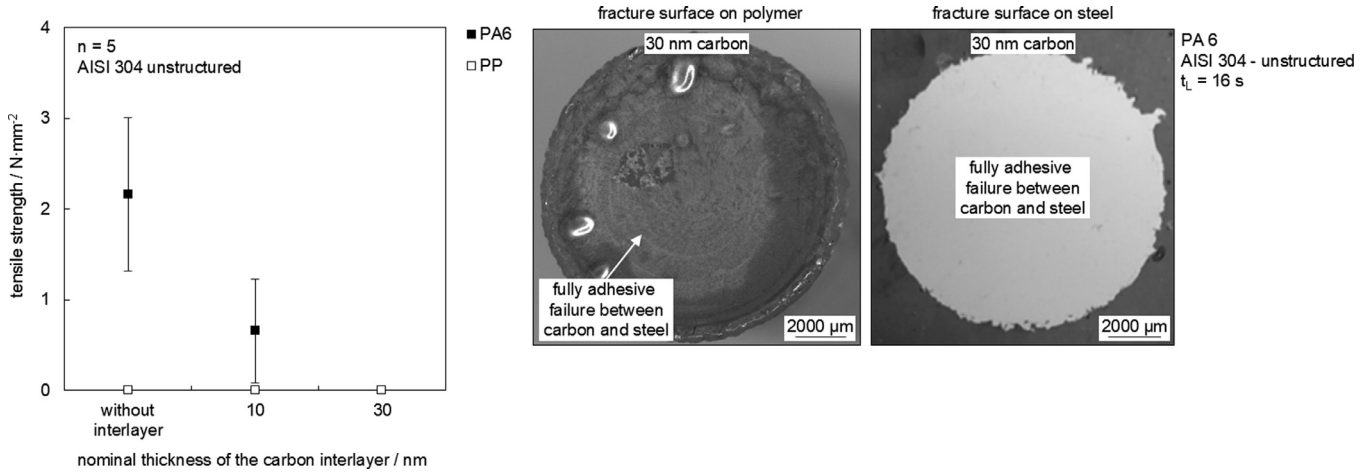

Fig. 10. Effect of carbon interlayers on tensile strength and fracture pattern.

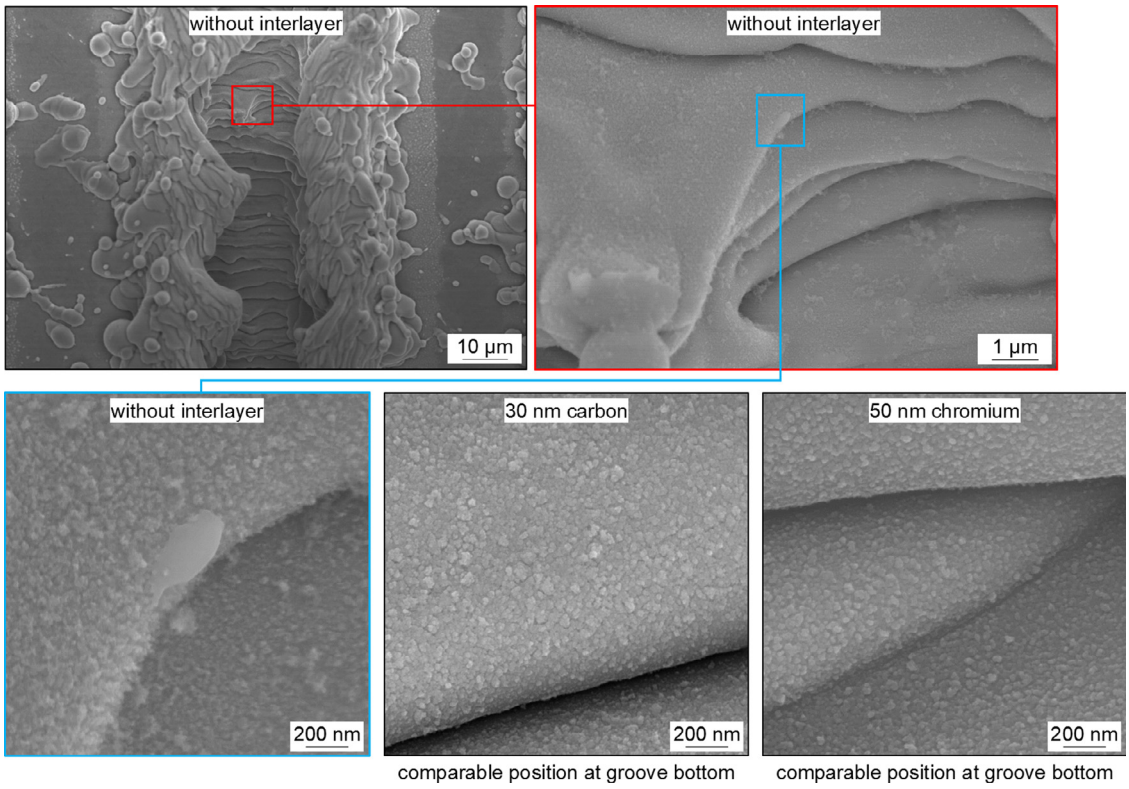

Fig. 11. Surface structures in SEM and appearance of different coatings at groove bottom.

Interaction between interlayers and surface preparation

Laser structuring significantly changes the surface topography of the metal. The surface is greatly enlarged, very fissured and undercuts are formed by the ejection of molten and recast metal. Fig. 11 shows the metal surface after laser material processing. In addition to the mentioned effects, even at low magnification, a scaly surface on the bottom of the groove can be detected, which is due to the pulsed processing and correlates with the pulse frequency of 60 kHz respectively a distance between each pulse in feed direction of approx. 5 µm. The large increase in surface area is not only a result of the macroscopic geometry. This is exemplarily given by the bottom of the groove (Fig. 11). At high magnification it can be seen that the surface is strongly roughened and not ideally smooth, it shows local, nanoscale elevations and deepenings. It follows that there are numerous possibilities for interlocking between molten plastic and metal on different scales.

If the interlayers consisting of chromium and carbon shown are to be used furthermore, their interaction with the surface structure must be specified. Firstly, it must be clarified whether the layers are present in the surface structures, secondly, whether they are continuous and thirdly, what impact is exerted on the topography. Only if there are reproducible conditions within the structures, the adhesion forces can be increased or set to zero in order to achieve a separation between firmly bonding and form fit.

Macroscopically there is no difference between coated and uncoated specimens, i.e. the grooves are similar. Fig. 11 shows the groove bottom also for the 30 nm thick carbon interlayer and for the 50 nm thick chromium interlayer at a comparable position to the uncoated sample.

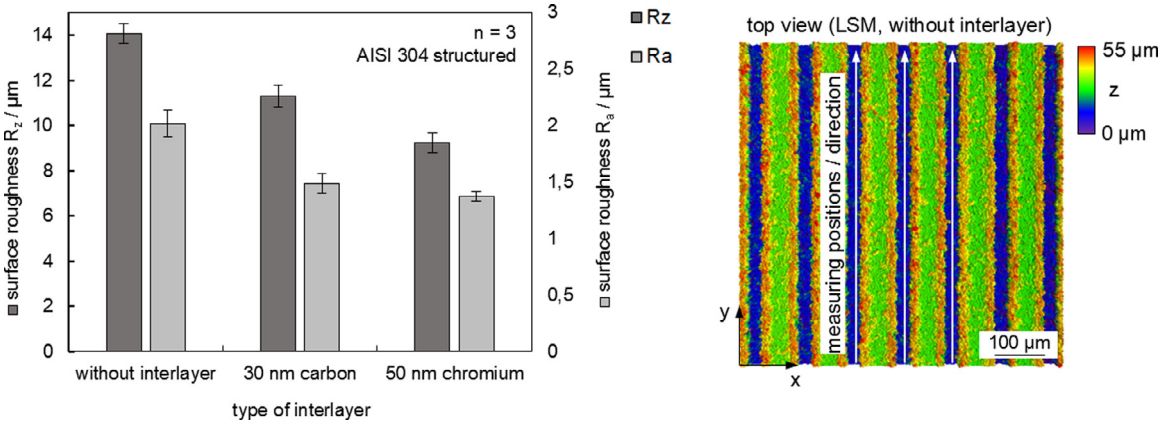

Fig. 12. Surface roughness of the groove bottom depending on different interlayers.

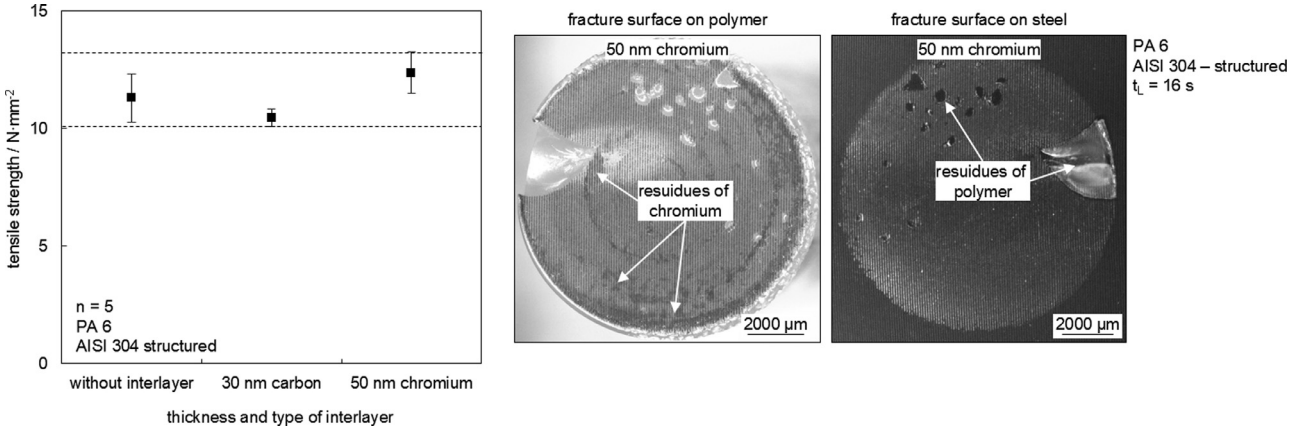

Fig. 13. Tensile strength of structured specimens depending different interlayers and exemplary fracture surfaces.

Table 4
Mean proportion of main alloying elements in the near-surface area.

Element	Unstructured reference (at.%)	In the structure / groove bottom (at.%)
Fe	65.08	57.24
Cr	23.76	35.45
Ni	7.74	2.51

On the nanoscale, the changed surface appearance compared to the uncoated base material shows that the carbon and chromium layers are continuously formed. Also, the transition between the single patterns at the scaly surface is still well reached by the layer. The layers for carbon and chromium appear comparable in the SEM pictures. In the case of the chrome coating, it is noticeable that a different morphology develops than on the unstructured base material (Fig. 8). This could be related to a change in the chemical composition of the surface caused by the laser beam process. Energy dispersive X-ray microanalysis (EDX) shows a significant increase in chromium content (Table 4). These changes in surface chemistry as well as in surface topography due the laser process can affect the structure of the resulting layers during the coating process (Hallmann and Ulmer, 2013; Mattox, 1996).

Optically it seems to come to a smoothing of the substrate, since the surface appears more evenly. This is also supported by the measurements of the roughness in the grooves by LSM (Fig. 12). The standard roughness values $R_z$and $R_a$were measured on the groove bottom. The comparison of the uncoated reference to the carbon- and chromium-coated samples shows that the roughness decreases significantly. Due to the optical measurement, however, these values only serve as an indication for the smoothing. Therefore, the trend between the different specimens rather than the absolute value will be considered.

Interaction between firmly bonding and form fit

In order to distinguish the components of firmly bonding and form fit within the bonding mechanism, the investigations are now carried out on structured samples. These are examined using the described carbon and chromium coatings. Fig. 13 compares the tensile strength of the uncoated reference to the carbon and chromium interlayers. The mean tensile strength of the reference is 11.3 ± 1.0 MPa, 10.5 ± 0.4 MPa using the carbon interlayer and 12.4 ± 0.9 MPa using the chromium interlayer. Considering the standard deviation, however, no clear difference can be found between the test series with different interlayers. In all cases considered, a mixed fracture with adhesive and cohesive fracture components was observed again (Fig. 13). If, however, the chromium and carbon interlayers were individually compared, an effect could be assumed. For this reason, the investigations were also carried out again with PA 12. In the case of unstructured surfaces with a 50 nm thick chromium interlayer, the tensile strength increases from approx. 2.2 MPa (without interlayer) to approx. 7.0 MPa (with interlayer) which is comparable to PA 6 (see chapter 3.2). For the application of structured samples, a chromium interlayer even reduced the mean tensile strength for PA 12-AISI 304 joints from 13.9 ± 0.5 MPa to 13.1 ± 0.9 MPa. In contrast, the tensile strength using the carbon interlayer remained constant at 14.0 ± 0.7 MPa with a slightly increased standard deviation. As with PA 6, the standard deviation also overlaps, which is why no

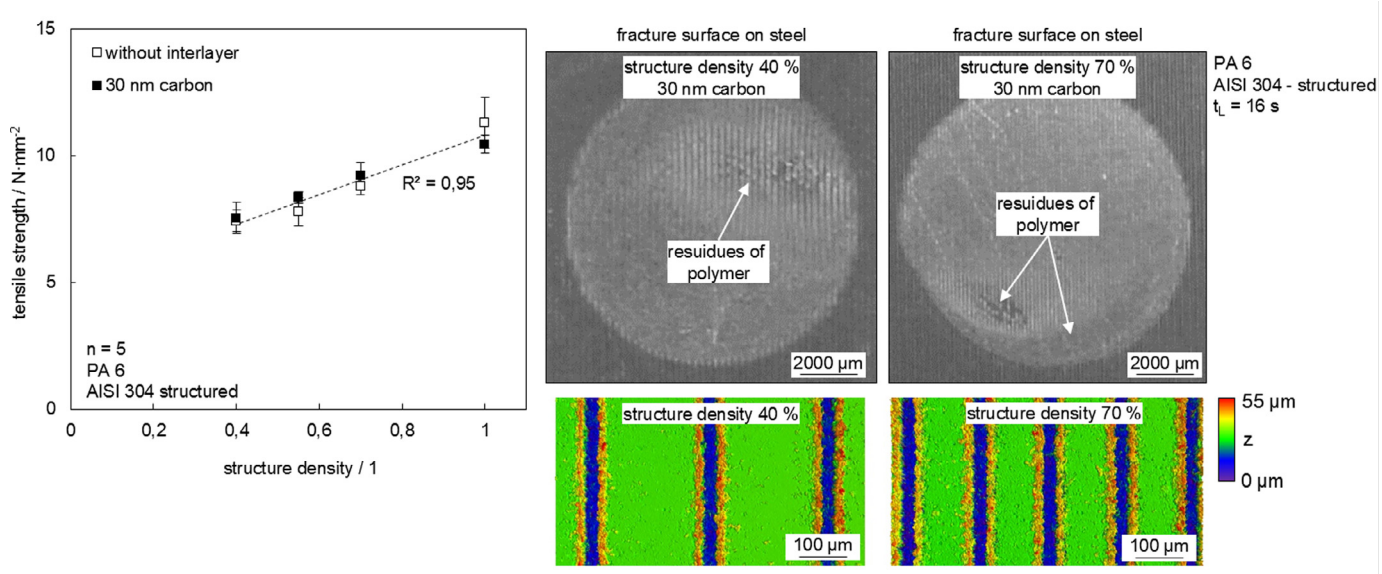

Fig. 14. Tensile strength depending structure density and carbon interlayer as interaction barrier.

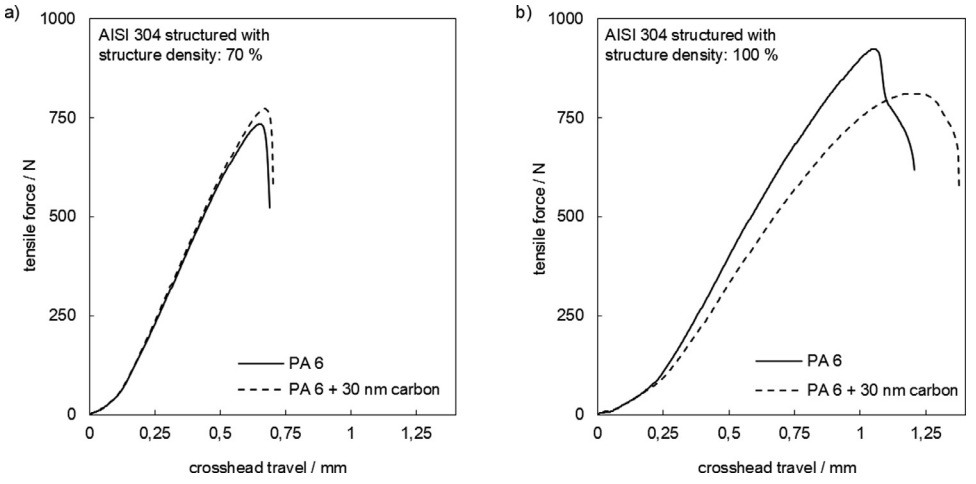

Fig. 15. Tensile force-crosshead travel graphs for structure densities 70% (a) and 100% (b) with and without using carbon interlayer as interaction barrier.

significant influence of the firmly bonding on the tensile strength can be determined.

Since the structure density can have a decisive influence on the form fit, this is to be evaluated conclusively. For this purpose, the distance between individual grooves was increased to adjust the number of structures per area unit. The structure density refers to the so far used surface structures as 100%. Fig. 14 shows the strength curve over the structural density with and without carbon interlayer. The tensile strength increases from approx. 7.5 MPa at 40% structure density to approx. 11 MPa for the reference structure. Within this interval, there is a linear relationship between achievable tensile strength and structure density. The linear regression reaches a 95% coefficient of determination. Given that a mixed fracture occurs with adhesive and cohesive fracture components for all considered structure densities (Fig. 14), this appears to be feasible. A plateau should only be reached if there is a complete cohesive failure of the plastic, which is probably too far away for the areas under consideration. This proves that the form fit scales with the increase in surface structures. By using the carbon interlayer as interaction barrier, it can also be demonstrated that the firmly bonding does not contribute significantly to the tensile strength, even at low structure densities. This clearly identifies the form fit as the decisive bonding mechanism. These studies were also referenced to PA 12 and were similarly confirmed.

This can also be seen in the force-crosshead travel curves of the joints. Fig. 15 shows two characteristic curves each for a structure density of 70% (a) and 100% (b) with and without interaction barrier. The behavior of the composite with regard to maximum force and crosshead travel is comparable in both cases. A failure of the metal-polymer joint with larger crosshead travels, which could indicate a greater ductility of the composite by a material closure, cannot be determined with this either.

Conclusions

In this article, hybrid composites between polymers (PA 6, PP) and AISI 304 were investigated. Starting from a description of the joining zone between the materials and ensuring a uniform connection between both joining partners, further investigations on the bonding mechanism were carried out. Therefore, the joint configuration allows tensile tests to be performed out in order to compare different surface conditions. Unstructured and structured sheet metals were used for this purpose. In order to distinguish the percentage of form fit and firmly bonding in the bonding mechanism, structured and unstructured sheets were used as joining partners. Starting with unstructured samples, the use of chromium interlayers allows an increase in adhesion forces through the production of chromium oxides, whereas the use of carbon

interlayers can eliminate them completely. These coatings were transferred to structured sheets. It is shown that the firmly bonding has no significant effect on the achievable tensile strength of the hybrid joint. These investigations were referenced with PA 12 and confirmed by an investigation of the achievable tensile strength at different structure densities. In all cases, the form fit was the decisive bonding mechanism regarding tensile strength.

Further investigations will address the effect of the bonding mechanism on other properties of the composite, e.g. tightness, and its durability. Further work will be carried out to quantify the force fit and its time-dependent effect on the joint.

Declaration of Competing Interest

The authors declare that they have no known competing financial interests or personal relationships that could have appeared to influence the work reported in this paper

Acknowledgement

The authors would like to thank Joachim Döll and the Institute of Micro- and Nanotechnologies MacroNano® at Technische Universität Ilmenau for the support during the experimental investigations as well as Jens Liefeith (M.Eng.) for the fruitful discussion.

References

Ageorges, C., Ye, L., 2001. Resistance welding of metal/thermoplastic composite joints. J. Thermoplast. Compos. Mater. 14 (6), 449–475.

Amancio-Filho, S.T., Bueno, C., dos Santos, J.F., Huber, N., Hage Jr., E., 2011. On the feasibility of friction spot joining in magnesium/fiber-reinforced polymer composite hybrid structures. Mater. Sci. Eng. A 528, 3841–3848 S.

Amend, P., Mohr, C., Roth, S., 2014. Experimental investigations of thermal joining of polyamide aluminium hybrids using a combination of Mono- and Polychromatic radiation. Phys. Procedia 56, 824–834.

Arai, S., Kawahito, Y., Katayama, S., 2014. Effect of surface modification on laser direct joining of cyclic olefin polymer and steel. Mater. Des. 59, 448–453.

Bergmann, J.P., Stambke, M., 2012. Potential of laser-manufactured polymer-metal hybrid joints. Phys. Procedia 39, 84–91.

Cenigaonaindia, A., Liébana, F., Lamikiz, A., Echegoyen, Z., 2012. Novel strategies for laser joining of polyamide and AISI 304. Phys. Procedia 39, 92–99.

Flock, D., 2011. Wärmeleitungsfügen hybrider Kunststoff-Metall-Verbindungen. Rheinisch-Westfälische Technische Hochschule Aachen, PhD thesis.

Hallmann, L., Ulmer, P., 2013. Effect of sputtering parameters and substrate composition on the structure of tantalum thin films. Appl. Surf. Sci. 282, 1–6.

Heckert, A., Zaeh, M.F., 2014. Laser surface pre-treatment of aluminium for hybrid joints with glass fibre reinforced thermoplastics. Phys. Procedia 56, 1171–1181.

Hino, M., Mitooka, Y., Murakami, K., Urakami, K., Nagase, H., Kanadani, T., 2011. Effect of aluminum surface state on laser joining between 1050 aluminum sheet and polypropylene resin sheet using insert materials,. Mater. Trans. 52 (5), 1041–1047 Nr.

Jung, D.-J., Cheon, J., Na, S.-J., 2016. Effect of surface pre-oxidation on laser assisted joining of acrylonitrile butadiene styrene (ABS) and zinc-coated steel. Mater. Des. 99, 1–9.

Katayama, S., Kawahito, Y., Niwa, Y., Kubota, S., 2007. Laser-Assisted metal and plastic joining. In: Proceedings of the LANE 2007: Laser Assisted Net Shape Engineering, 5, pp. 41–51.

Katayama, S., Kawahito, Y., 2008. Laser direct joining of metal and plastic. Scr. Mater. 59, 1247–1250.

Kawahito, Y., Katayama, S., 2010. Characteristics of LAMP joining structures for several materials. In: Proceedings of 29th International Congress on Applications of Laser & Electro-Optics, pp. 1469–1473.

Krevelen, D.W.van, Nijenhuis, K.T., 2009. Properties of Polymers: Their Correlation With Chemical Structure; Their Numerical Estimation and Prediction from Additive Group Contributions. Elsevier, Amsterdam Fourth, completely revised edition.

Kohl, M.-L., Schricker, K., Bergmann, J.P., Lohse, M., Hertel, M., Füssel, U., 2018. Thermal joining of thermoplastics to metals: surface preparation of steel based on laser radiation and tungstern inert gas arc process. Procedia CIRP 74, 500–505.

Lamberti, C., Solchenbach, T., Plapper, P., Possart, W., 2014. Laser assisted joining of hybrid polyamide-aluminum structures. Phys. Procedia 56, 845–853.

Lee, L.-H. (Ed.), 1991. Fundamentals of Adhesion Springer Science+Business Media, New York.

Markovits, T., Bauernhuber, A., Géczy, M., 2012. Investigating the shape locking phenomenon in case of LAMP joining technology. Phys Procedia 39, 100–107.

Mattox, D.M., 1996. Surface effects on the growth, adhesion and properties of reactively deposited hard coatings. Surf. Coat. Technol. 81, 8–16.

Paul, H., Luke, M., Henning, F., 2014. Kunststoff-Metall-Hybridverbunde - Experimentelle Untersuchungen zum Verformungs- und Versagensverhalten. Zeitschrift Kunststofftechnik 10, 118–141.

Schricker, K., Stambke, M., Bergmann, J.P., Bräutigam, K., Henckell, P., 2014. Macroscopic surface structures for polymer-metal hybrid joint manufactured by laser based thermal joining. Phys. Procedia 56, 782–790.

Schricker, K., Stambke, M., Bergmann, J.P., 2015. Experimental investigations and modeling of the melting layer in polymer-metal hybrid structures. Welding in the World 59, 407–412.

Schricker, K., Stambke, M., Bergmann, J.P., Bräutigam, K., 2016. Laser-Based joining of thermoplastics to metals: influence of varied ambient conditions on joint performance and microstructure. Int. J. Polym. Sci. 9, 2016.

Schricker, K., Bergmann, J.P., 2018. Determination of sensitivity and thermal efficiency in laser assisted metal-plastic joining by numerical simulation. Procedia CIRP 74, 511–517.

Schricker, K., Diller, S., Bergmann, J.P., 2018. Bubble formation in thermal joining of plastics with metals. Procedia CIRP 74, 518–523.

Schricker, K., Bergmann, J.P., 2019. Temperature- and Time-Dependent penetration of surface structures in thermal joining of plastics to metals. Key. Eng. Mater. 809, 378–385.

Tan, X., Shan, J., Ren, J., 2013. Effects of Cr plating layer on shear strength and interface bonding characteristics of mild steel/CFRP joint by laser heating. Acta Metallurgica. Sinica. 49 (6), 751–756 Nr.

Zhang, Z., Shan, J.-G., Tan, X.-H., Zhang, J., 2016. Effect of anodizing pretreatment on laser joining CFRP to aluminum alloy A6061. Int. J. Adhesion and Adhesives 70, 142–151.